Neuron
Article

# Representations of Odor in the Piriform Cortex

Dan D. Stettler[1] and Richard Axel[1,*]
[1]Department of Neuroscience and Howard Hughes Medical Institute, College of Physicians and Surgeons, Columbia University, New York, NY 10032, USA
*Correspondence: ra27@columbia.edu
DOI 10.1016/j.neuron.2009.09.005

## SUMMARY

**Olfactory perception is initiated by the recognition of odorants by a large repertoire of receptors in the sensory epithelium. A dispersed pattern of neural activity in the nose is converted into a segregated map in the olfactory bulb. How is this representation transformed at the next processing center for olfactory information, the piriform cortex? Optical imaging of odorant responses in the cortex reveals that the piriform discards spatial segregation as well as chemotopy and returns to a highly distributed organization in which different odorants activate unique but dispersed ensembles of cortical neurons. Neurons in piriform cortex, responsive to a given odorant, are not only distributed without apparent spatial preference but exhibit discontinuous receptive fields. This representation suggests organizational principles that differ from those in neocortical sensory areas where cells responsive to similar stimulus features are clustered and response properties vary smoothly across the cortex.**

## INTRODUCTION

Olfactory perception requires the recognition of odorants by receptors in the periphery and more central mechanisms in the brain that process this information to allow for the discrimination of odorants. Individual sensory neurons in mice express only one of 1500 different receptor genes (Buck and Axel, 1991; Zhang and Firestein, 2002; Godfrey et al., 2004). An odorant can interact with multiple distinct receptors, resulting in the activation of an ensemble of sensory neurons (Malnic et al., 1999; Araneda et al., 2004; Oka et al., 2006). Discrimination among odorants then requires that the brain determine which of the sensory neurons have been activated by a given odorant. Neurons expressing a given receptor, although randomly distributed within zones of the epithelium, project with precision to two spatially invariant glomeruli in the olfactory bulb (Vassar et al., 1993, 1994; Ressler et al., 1993, 1994; Mombaerts et al., 1996). Thus, a transformation in the representation of olfactory information is apparent in the bulb where the randomly distributed population of active neurons in the sense organ is consolidated into a discrete spatial map of glomerular activity.

What is the nature of the representation in the bulb and in the next olfactory processing center, the piriform cortex? In the visual, auditory, and somatosensory systems, spatial information in the peripheral sense organs is maintained in the sensory cortex (Woolsey and Walzl, 1942; Talbot and Marshall, 1941; Marshall et al., 1941). In these sensory neocortices, cells responsive to similar stimulus features are clustered, and response properties vary smoothly across the cortex. In the olfactory bulb, imaging experiments reveal that different odorants elicit distinct spatial patterns of glomerular activity (Rubin and Katz, 1999; Johnson and Leon, 2000; Uchida et al., 2000; Meister and Bonhoeffer, 2001; Wachowiak and Cohen, 2001; Spors and Grinvald, 2002; Xu et al., 2003; Lin et al., 2006; Soucy et al., 2009). These studies reveal a coarse chemotopic representation; glomeruli responsive to structurally similar odorants are spatially segregated within domains, but within these domains glomeruli with differing odorant specificities are interspersed.

The representation of odorants in the piriform has been examined by electrophysiological recordings, imaging of intrinsic signals, and analysis of odorant evoked Fos gene expression (Rennaker et al., 2007; Sugai et al., 2005; Illig and Haberly, 2003; Poo and Isaacson, 2009). The mitral and tufted cells, the output neurons of the bulb, extend an apical dendrite into a single glomerulus and project axons to several telencephalic areas and provide significant input onto pyramidal neurons of the piriform cortex (Price and Powell, 1970). Mitral cell axons synapse with dendrites of pyramidal cells in layer 1 of piriform, a three-layered paleocortex. Electrophysiological recordings of individual pyramidal cells at several positions in the anterior piriform cortex reveal cells responsive to a given odorant distributed across the cortex (Rennaker et al., 2007). However, efforts to examine the spatial structure of cortical activity in the piriform cortex by recording a small number of widely separated cells may not permit the detection of patterned neural activity. More extensive sampling of cortical activity derives from analysis of Fos gene expression (Illig and Haberly, 2003). These studies reveal that cells responsive to an odorant are dispersed without obvious spatial pattern, but Fos imaging permits detection of the response of cells to only a single odorant and depends upon an interpretation of the source of the Fos signal.

We have therefore visualized odorant representations in piriform by optically recording the responses of large populations of neurons across the cortex at single-cell resolution. These studies reveal that the piriform does not exhibit a pattern of neural activity in which cells respond to a given odorant with great selectivity. Rather, the specificity of an odorant appears to be represented by unique and distributed ensembles of neurons that no longer display the coarse chemotopy or spatially segregated patterns of neural activity observed in the olfactory

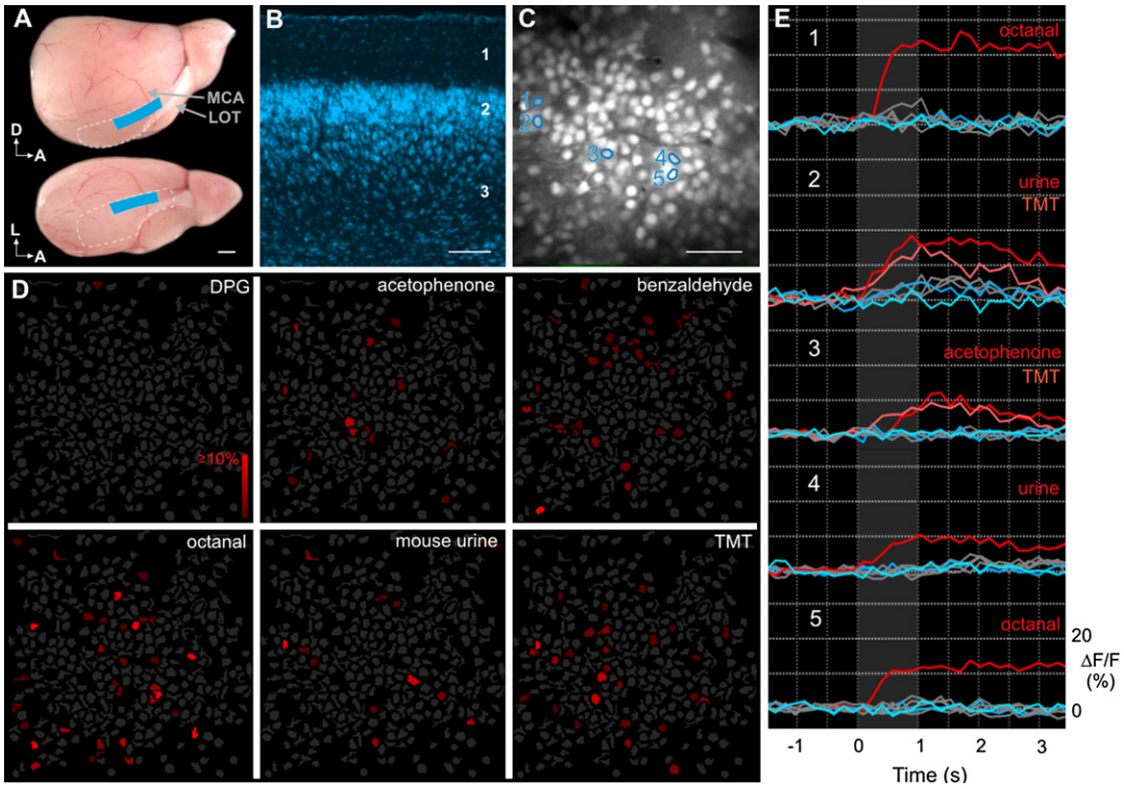


**Figure 1. Odorant-Evoked Responses in Mouse Piriform Using In Vivo Two-Photon Calcium Imaging**

(A) Views of the lateral (top) and ventral lateral (bottom) surface of the mouse cerebral hemisphere showing the piriform cortex outlined by a white dotted line. The imaged area is highlighted in blue. The same region of piriform was imaged in different animals using the middle cerebral artery (MCA) and lateral olfactory tract (LOT) as landmarks. Scale = 1 mm.

(B) Coronal slice of piriform showing the characteristically dense layer 2, which is occupied primarily by the somata of pyramidal cells that receive direct input from the bulb upon their apical dendrites in layer 1. Neuronal nuclei were labeled using NeuroTrace. Scale = 100 μm.

(C) Baseline fluorescence of cells in layer 2 loaded with Oregon Green 488 BAPTA-1 AM and imaged in vivo with two-photon microscopy. Scale = 50 μm.

(D) The cells in panel (C) were identified by custom software using their baseline fluorescence and were overlayed with cellular responses to odorants presented in gradations of red corresponding to the level of response. Di(propylene glycol) (DPG) is used to dilute odorants to approximately equal concentration (3 ppm in air). Five structurally diverse odorants, including the complex odorant, female mouse urine, activate dispersed subsets of cells. 2,5-dihydro-2,4,5-trimethylthiazoline (TMT), a component of fox urine that elicits innate aversive behavior in the mouse, also activates cells in this region.

(E) Traces depicting changes in fluorescence elicited by the five odorants for the five cells outlined in (C). Adjacent cells can respond selectively to different odorants. The traces of odorants not eliciting a response are gray, and those of DPG and air are blue.

bulb. This representation suggests organizational principles that differ from those in neocortical sensory areas where cells with similar receptive fields are clustered and tuning varies smoothly across the cortex. These data suggest a model in which connections from bulb to cortex involve random, convergent, excitatory inputs to piriform cells, a feature that may render the piriform a purely associative cortex.

## RESULTS

### Odorant-Evoked Responses in Piriform Cortex

We have developed procedures that permit the recording of odorant-evoked changes in fluorescence intensity in neurons of the piriform cortex in mice by two-photon microscopy (Denk et al., 1990). The piriform cortex is a three-layered structure on the ventral lateral surface of the cerebral hemisphere (Figure 1A). The major projection neurons of the piriform cortex, the pyramidal cells, locate their cell bodies in layers 2 and 3 and extend apical dendrites to layer 1 where they synapse with mitral cell afferents from the olfactory bulb (Figure 1B). A surgical procedure was developed to expose the ventral surface of the temporal lobe, rendering the piriform cortex optically accessible to two-photon microscopy. Piriform neurons were loaded with the calcium-sensitive fluorescent dye, Oregon Green 488 BAPTA-1 AM, by injection of dye into broad regions of layer 1 (Stosiek et al., 2003; Ohki et al., 2005). This bulk-loading technique led to the efficient uptake of dye by the dendrites and the labeling of greater than 90% of the pyramidal cell bodies in layers 2 and 3 across wide regions of the piriform cortex (Figure 1C). This preparation maintains the integrity of the olfactory system and reveals odorant-evoked changes in fluorescence intensity in pyramidal cells for as long as 12 hr.

We imaged odorant responses at multiple sites in over 100 animals. We present typical examples that illustrate the features

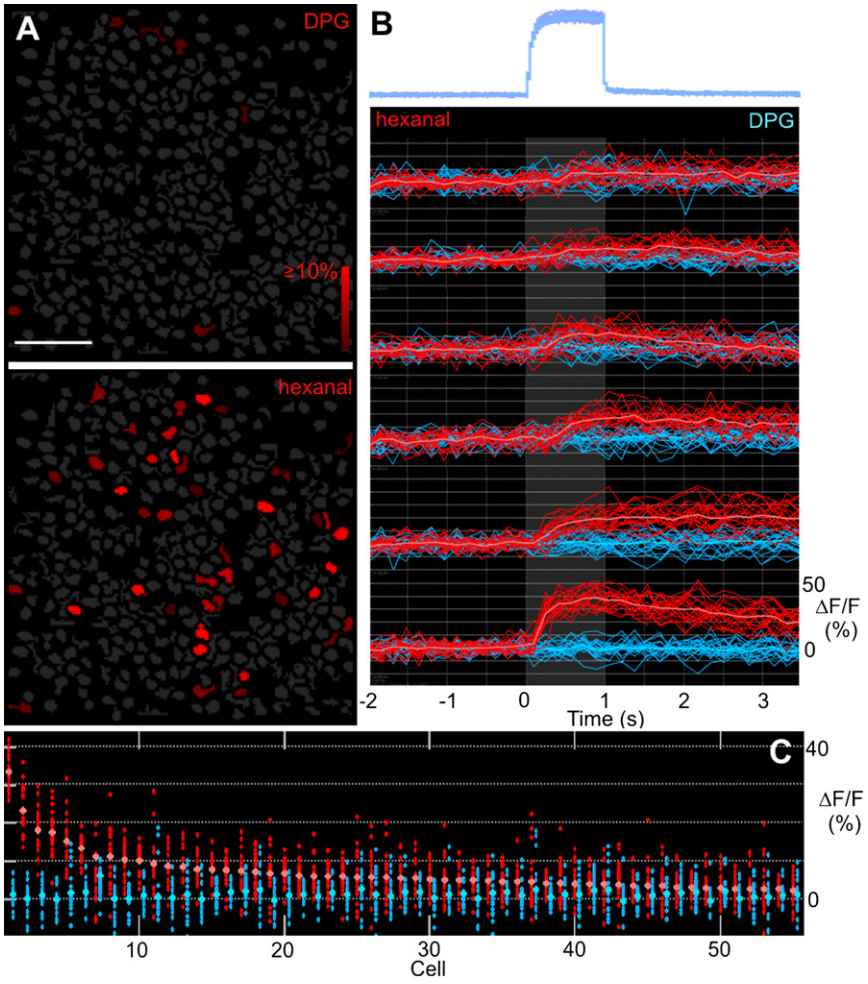


**Figure 2. Odorant-Evoked Calcium Responses in Piriform Cortex Are Highly Consistent**

(A) Responses to DPG and hexanal are superimposed upon an image of identified cells. Fifty-five of 335 cells in this field exhibit significant increases in fluorescence when the animal is stimulated with hexanal. Scale = 50 μm.

(B) The superimposed traces from 20 sequentially delivered odorant pulses measured using a photoionization detector are shown at the top in blue. The superimposed fluorescence traces from 20 hexanal (red) or DPG (blue) trials are presented below for six different cells along with the cross-trial average for each cell. The individual trial traces are highly consistent, even for those cells with small responses.

(C) The average ΔF/F for the 2 s epoch after the onset of hexanal (red) or DPG (blue) delivery is shown for all 20 trials for the 55 cells identified as responding to hexanal. Single-trial hexanal responses are distributed monomodally around the cross-trial average, shown in pink.

of odorant-evoked responses in the piriform. We have analyzed responses in multiple animals to determine the variability of these features. Stimulation consisted of a 1 s puff of odorant in diluted concentrations ranging from 0.5 to 80 ppm in air. Prestimulation images acquired upon exposure to air were used to calculate the baseline fluorescence of labeled pyramidal cells. Responses reflect a cell-based analysis of aligned images corrected for movement (Figures S1 and S2). Exposure to 20 different odorants, at concentrations from 0.5 to 80 ppm, elicited fluorescence changes in 3%–15% of the piriform neurons (Figures 1D and 1E). Each odorant activated a unique ensemble of cells in layer 2 (Figure 1D). The frequency of responding cells differed for different odorants but was consistent for each odorant across multiple fields in different animals. When presented at 3 ppm, for example, octanal activated 10.2% of the labeled piriform cells (±1.1 SEM, n = 14 animals; for c = 16967 cells in f = 45 imaging fields), whereas α-pinene activated 6.5% (±1.0 SEM, n = 6, c = 9297, f = 21) and benzaldehyde activated only 3.3% (±0.8 SEM, n = 3, c = 2982, f = 10) of the piriform cells. Odorant-evoked responses in fields of ~300 cells were consistent across multiple trials: on average, a cell responsive to a given odorant was activated in over 80% of 15 trials (Figures 2 and S3). This consistency is similar to calcium responses measured in rodent visual cortex but much greater than the variable responses recently observed in barrel cortex (Ohki et al., 2005; Kerr et al., 2007). Moreover, the responses were eliminated by blockade with the glutamate antagonists, CNQX and APV, indicating that the observed responses were synaptically mediated (Figure S4).

Cells responsive to a given odorant within the same imaging field exhibited a range of statistically significant positive responses, with ΔF/F values between 2% and 50%. In a field of 300 cells in which 55 neurons responded to one of six odorants, 47 cells exhibited a ΔF/F below 10%, whereas eight cells exhibited a ΔF/F from 10%–40% (Figures 2A and 2C). This skewed distribution of response intensities could reflect different levels of convergent input from active mitral cells, a property that could follow an exponential distribution consistent with our data.

The response to increasing odorant concentrations in the piriform was subadditive and saturating. As the octanal concentration was increased from 3 to 80 ppm, the frequency of responsive cells approached saturation at a value of 20% active cells. At 3 ppm, 10% of the cells were activated, and this value only increased to 20% at 25-fold higher odorant concentrations (Figure 3). Most cells exhibited subadditive increases in intensity with increasing odorant concentration, but one-third of the cells exhibited a decline in activity at higher concentration. The presence of a population of cells that exhibited diminished response intensities as odorant concentration was increased suggests that suppression accompanies increases in activity, a conclusion further supported by experiments with odorant mixes (see below).

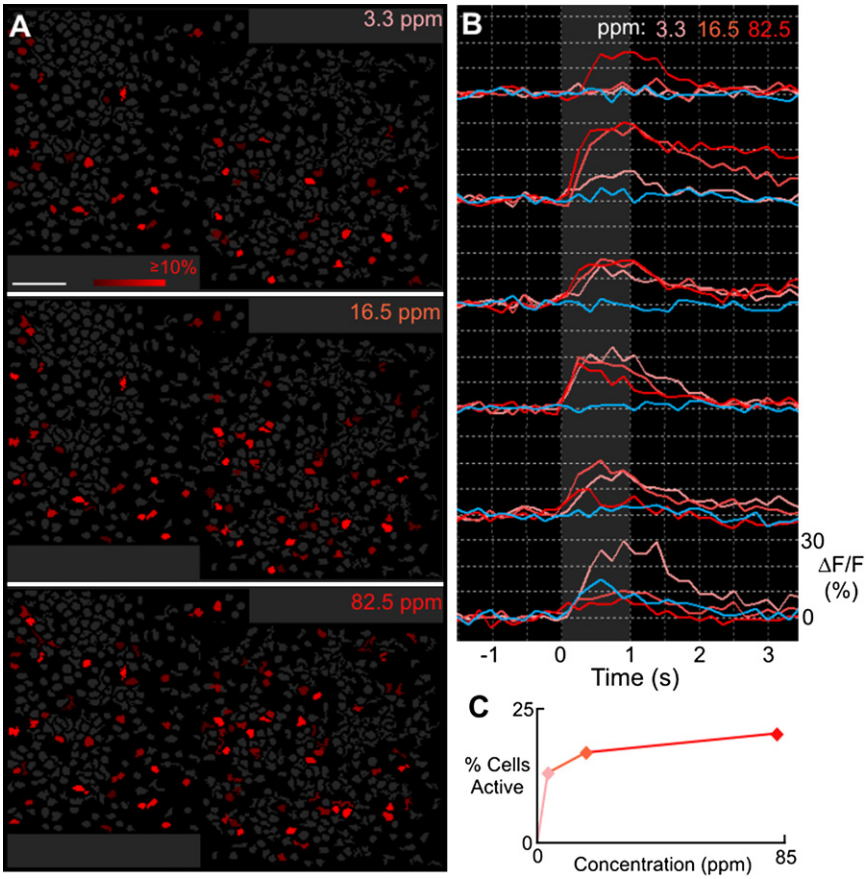


**Figure 3. Concentration Dependence of Odor-Evoked Responses**

(A) Graded maps showing responses to octanal at concentrations (in ppm) indicated in the upper right corner of each panel. At 3.3 ppm, 12% of the cells are activated, and this value only increases to 20% at 82.5 ppm, a 25-fold higher odorant concentration. Scale = 50 μm.

(B) Most cells exhibit nonlinear increases in intensity with increasing odorant concentration, but one-third of the cells exhibit a decline in activity at higher concentration.

(C) The frequency of responsive cells is nonlinear as a function of octanal concentration and saturates at a value of 20% active cells.

## Different Odorants Activate Unique Ensembles of Neurons

Each odorant activated a population of from 3% to 15% of the neurons in layer 2 of the piriform cortex. The responses of individual cells could be resolved, and adjacent cells responsive to different odorants were readily distinguished (Figures 1C and 1E). Within a single imaging field, cells responsive to a given odorant were dispersed rather than clustered, and cells responding to different odorants were therefore intermingled. Cells adjacent to an octanal-responsive neuron, for example, were equally likely to respond to 2,5-dihydro-2,4,5-trimethylthiazoline (TMT, an aversive fox odorant) or female mouse urine (an attractive odorant) as they were to octanal (Figures 1C–1E). No spatial clustering of neurons responsive to a given odorant could be discerned within localized imaging fields.

Each odorant activated a distinct ensemble of cortical neurons. Individual cells within the ensemble could respond to multiple structurally dissimilar odorants. 12.8% of the cells responsive to octanal, for example, were also responsive to α-pinene (±2.7 SEM, n = 6 animals), and about 9.0% of octanal-responsive cells also responded to butyric acid (±1.3 SEM, n = 3; Figures 4A and 4B). A given neuron in piriform cortex responded to multiple dissimilar odorants and therefore exhibited what might be called a "discontinuous" receptive field. These observations imply that the identity of an odorant cannot be determined by the activity of an individual neuron. Rather, an odorant is likely to be represented by an ensemble of active neurons that is unique to an individual odorant.

The distinct representations of structurally dissimilar odorants in cortex presumably reflect the observation that these odorants activate largely nonoverlapping sets of glomeruli in the olfactory bulb. However, structurally similar odorants such as octanal and hexanal, for example, activate glomerular populations with over 70% overlap (Meister and Bonhoeffer, 2001). In the piriform cortex, the patterns of active neurons elicited by these odorants exhibited 26.6% overlap (±2.0 SEM, n = 7; Figures 4C and 4D). This value is greater than the 5%–15% overlap typically observed between structurally distinct odorants but is far less than the overlap between the set of hexanal- and octanal-responsive glomeruli described in the bulb (Meister and Bonhoeffer, 2001). The extent of overlap between the representations of two odorants will change depending upon where the threshold is set, an inherent problem in imaging experiments. Increasing the threshold diminishes overlap, whereas lowering the response threshold increases overlap. The overlap between octanal and hexanal is not large even at low thresholds that maximize overlap. Thus, the overlapping representations of structurally similar odorants observed in the bulb are decorrelated in piriform cortex.

We also observed a small subset of cells that responded to the majority of odorants tested. In a typical experiment, in a given field of cortical neurons exposed to five structurally distinct odorants, about 35% of the neurons responded to at least one odorant, and only 2% of the neurons responded to four or five of the odorants (Figure 4B). The frequency of cells that responded promiscuously to multiple odorants was consistent across several imaged fields. These neurons may have input characteristics different from the vast majority of the responding piriform cells.

## The Spatial Distribution of Cortical Neurons Responsive to a Given Odorant

A given odorant activates a spatially stereotyped population of glomeruli in the olfactory bulb (Rubin and Katz, 1999; Belluschio

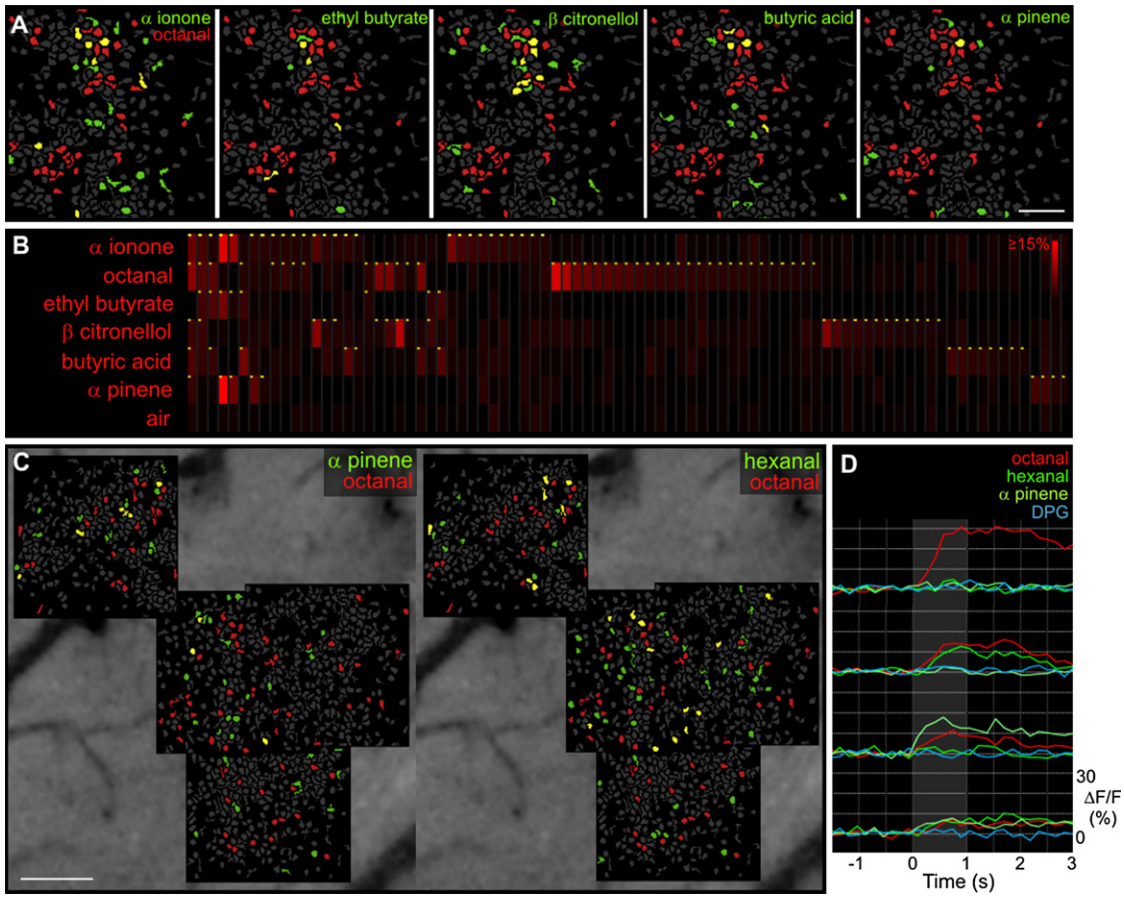


**Figure 4. Odorants Evoke Responses in Unique but Overlapping Ensembles of Piriform Neurons**

(A) Cells responsive to octanal (red) overlayed on the responses to five other odorants (green) in piriform layer 2. The cells are presented as either responsive or not responsive with no graded color code. Yellow cells respond to both odorants. Each odorant evokes responses in different but overlapping ensembles of piriform cells. Scale = 50 μm.

(B) Array showing the responses of cells from panel (A) to each of the six presented odorants. Only those cells responding to at least one odorant are shown. A yellow dot in the upper left corner of the cell/odorant pairing indicates a significant response. Approximately one-quarter of the cells respond to more than one odorant, but only six of the 85 cells respond to three or more odorants.

(C) Octanal (red) and α-pinene or hexanal (green) responsive cells in multiple adjacent imaging sites containing 972 labeled cells in layer 2 of the piriform cortex. The imaged sites are superimposed upon the blood vessels at the surface of the piriform that are used for alignment. Of the 88 cells responding to octanal, nine also respond to the structurally dissimilar odorant α-pinene, and 19 also respond to the highly similar odorant hexanal. Scale = 100 μm.

(D) Sample fluorescence traces for four cells from panel (C). Some cells respond strongly to octanal (top) or hexanal without responding even weakly to the other.

and Katz, 2001; Bozza et al., 2004; Soucy et al., 2009). Superimposed upon this invariant insular map is a coarse chemotopy such that structurally similar odorants often activate glomeruli in circumscribed regions of the olfactory bulb (Lin et al., 2006; Takahashi et al., 2004; Ingarashi and Mori, 2005). We imaged multiple overlapping fields to survey large areas of both the anterior and posterior piriform cortex to determine whether different odorants activated spatially segregated populations of cortical neurons. Imaging was performed on similar regions of piriform cortex in different individuals using the middle cerebral artery and the lateral olfactory tract as anatomic landmarks (Figure 5A). Optical recordings were obtained with 16 structurally diverse odorants across overlapping fields of 300 cells in about 100 animals. We present typical examples of this analysis in Figures 5 and S5–S8. Cells responsive to a given odorant were distributed throughout the entire imaged fields without evidence for segregation, with only incidental clustering that was not replicated across animals (Figure 5C). We found a similar distribution of responsive cells for each of 16 structurally distinct odorants independent of imaging location in piriform. These results are in accord with our observations upon imaging single fields and reveal the intermingling of cells responsive to different odorants.

The representations of odorants displayed no reliable patterning on a large (1 mm) or small (100 μm) spatial scale. No consistent patches of responsive cells or gradients in the density of responsive cells were observed across the imaged regions stretching 3 mm and encompassing as much as 20% of the piriform's area and 50% of its length. The density of responsive cells in the representation of a given odorant could vary 2- to 3-fold across spatial scales of hundred of microns (Figures 5C and

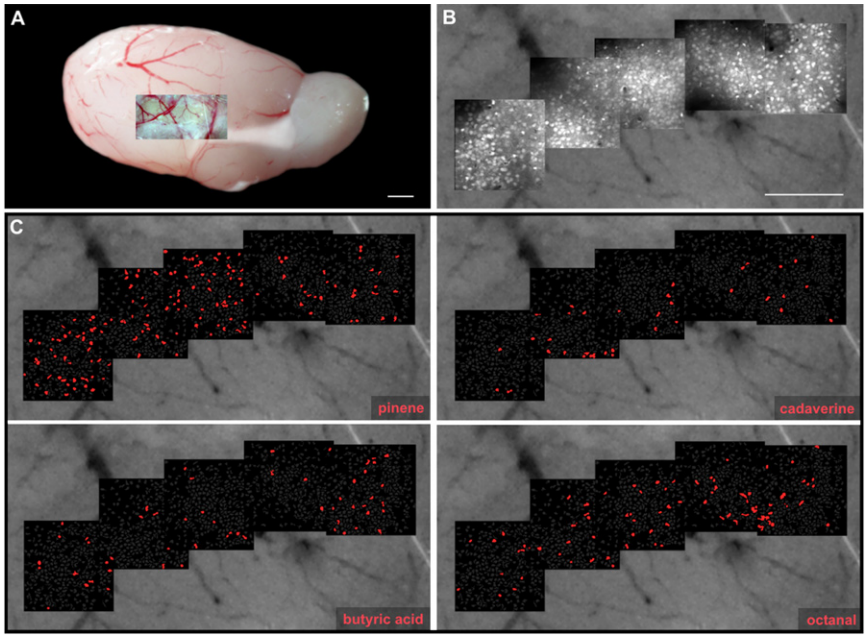


**Figure 5. Distributed Odorant Representations Extend across Wide Regions of Piriform Cortex**

(A) Ventral lateral view of a mouse cerebral hemisphere superimposed with the imaging craniotomy. The surface vasculature enables the montage of imaging sites positioned widely across the piriform and the determination of their location within the hemisphere. Scale = 1 mm.

(B) Montage of images showing the baseline fluorescence of labeled cells in five contiguous imaging sites across layer 2 of the piriform cortex in the hemisphere shown in panel (A). The montage overlies the vessels at the surface of the cortex that was used for alignment. The imaged region contains 1301 loaded cells. Scale = 200 μm.

(C) Responsive cells to four odorants across a wide region of piriform cortex shown in panel (B). The odorants were diluted to approximately the same concentration (3 ppm in air) except for α-pinene, which was presented at 15 ppm. Different odorants elicit different numbers of responsive cells. The density of responsive cells to a given odorant can vary three-fold over ranges of 100 μm.

S6–S8). Monte Carlo simulation in which we randomly distribute the same number of responsive cells on the same locations yielded similar results (Figure S9). However, autocorrelation analysis of the representations of individual odorants and cross-correlation analysis of the representations of different odorants revealed no periodic patterning that was consistent across animals (Figure S10). The distribution of responsive cells across the piriform does not change when we consider only the highest responding cells (ΔF/F > 5%; Figure S11). There was likewise no evidence for a graded spatial distribution of cells responsive to an odorant, a finding inconsistent with a rostral-caudal gradient of odorant responses reported for intrinsic imaging of the guinea pig piriform (Sugai et al., 2005).

The behavioral relevance of odorants also does not appear to be regionally mapped in piriform since cells responsive to two odorants that elicit opposing behaviors (mouse urine and a component of fox excretions, TMT) were intermingled. Thus, neither the spatially segregated patterns of active glomeruli nor the associated chemotopy observed in the olfactory bulb were found in the distributive odorant representations in piriform cortex. The absence of discernible patterning suggests the possibility that the cells' responsive to a given odorant may be randomly distributed in the piriform cortex.

## The Response of Piriform Cortex to a Mix of Odorants: Synergy and Suppression

Pyramidal neurons are thought to integrate convergent mitral cell input from multiple glomeruli onto individual pyramidal cells. This model predicts that exposure to a mix of two odorants will result in the activation of a significant subset of pyramidal neurons that are not activated by the individual components of the mix. Alternatively, if pyramidal neurons receive input from only a single glomerulus, the representation of an odorant mix should reflect the combined representations of the component odorants presented separately. We therefore exposed mice to either octanal, α-pinene, or hexanal alone or in pair-wise mixes and imaged across multiple fields in the piriform cortex (Figure 6). 20%–40% (average = 32.3% ± 3.7% SEM, n = 5 animals) of the neurons responsive to a mix did not respond to either of the individual components, a finding consistent with the convergence of inputs from multiple glomeruli (Figure 6A). However, the responses of the cells active only with a mix was on average weak (ΔF/F below 10%); this population did not include the subset of strong responses (ΔF/F above 10%) that were consistently observed with component odorants.

The most prominent feature observed with a mix was suppression. 40%–60% of the cells responsive to the individual components failed to respond to a mix of these components (average = 50.0% ± 3.5% SEM, n = 5 animals). In a field of 1039 cells in which 188 responded to octanal or α-pinene alone, we observed that only 120 responded upon exposure to the mix (Figure 6A). This suppression was observed for pair-wise combinations of structurally similar (octanal/hexanal) and dissimilar (octanal/pinene; octanal/ethyl methyl sulfide, data not shown) odorants. Moreover, suppression was not only reflected by the cells that responded to components and not to the mix but also by diminished responses in those cells that remained active to the mix (Figures 6B–6D). The extent of synergy or suppression a cell exhibited with a mix does not correlate with the magnitude of its response to a single component.

The observed suppression was not specific. α-pinene elicited an excitatory response in 4% of the piriform cells when presented alone, yet elicited suppression in over 90% of the octanal-responsive cells when presented in a mix. Thus, the representation of a mix of odorants in piriform retains features of the representations of the components and exhibits a small synergistic collection of cells, but its most prominent feature is strong, nonspecific inhibition.

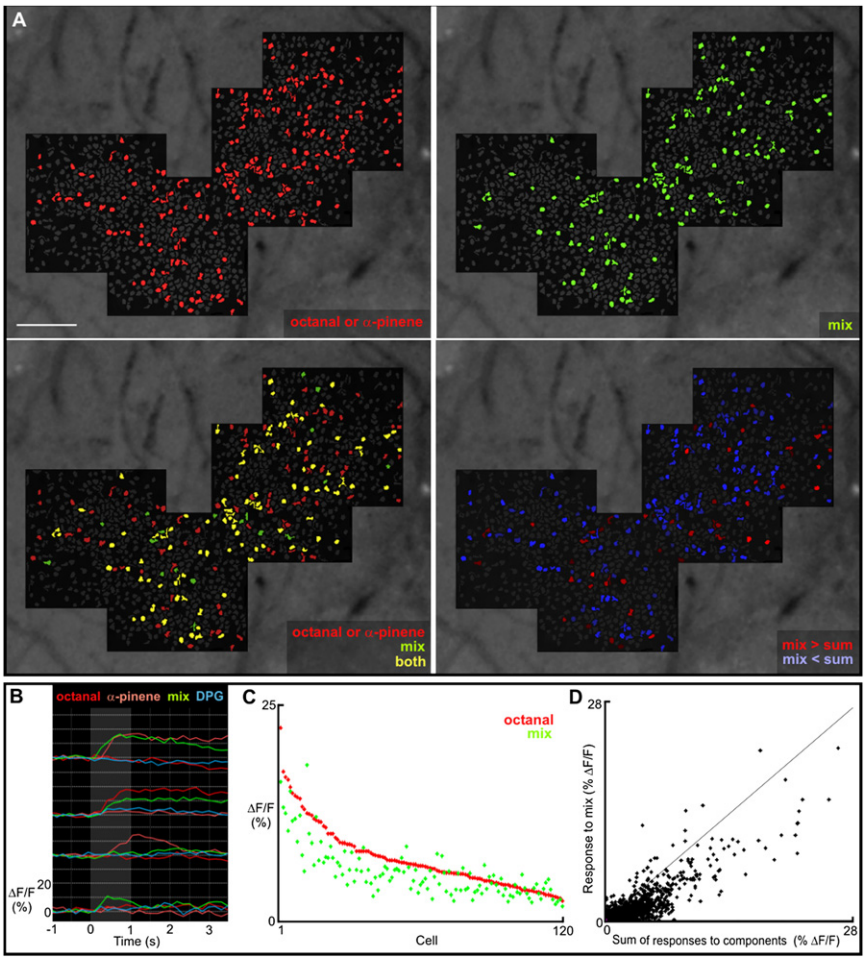


**Figure 6. The Response of Piriform Cells to a Mix of Odorants Exhibits Strong Suppression and Weak Synergy**

(A) Montage of four imaging sites from layer 2 of piriform cortex containing 1039 labeled cells. The red cells in the upper left panel respond to either octanal or α-pinene presented alone. The green cells in the upper right panel respond to a mix of octanal and α-pinene at the same concentration as used at the left. The overlap between the responses to the individual odorants and to the mix is shown in the lower left. Cells responsive to individual odorant alone and the mix are yellow. Cells responsive to odorant presented alone but not to the mix remain red, whereas cells responsive to the mix but not individual odorants are green. 36% of the 188 cells responsive to the individual odorants do not respond to the mix. The difference between the sum of the responses to the individual odorants and the response to the mix, with gradations of red indicating higher mix responses and gradations of blue indicating lower mix responses, is presented in the lower right. Scale = 100 μm.

(B) Sample traces from panel (A) showing a cell that exhibits a similar response to α-pinene and the mix (top), cells that exhibit a partially (second from top) or completely (third from top) suppressed response to the mix, and a cell that responds only to the mix (bottom). Cellular responses to mix alone are invariably weak.

(C) Ranked-ordered responses to octanal (red) and responses to the mix of octanal and α-pinene (green) shown for those cells that responded to octanal but not α-pinene. Data presented are for 2177 cells from the imaged fields shown in panel (A), as well as three additional, nonadjacent fields in the same animal.

(D) The sum of each cell's response to the individual odorants presented separately compared with the cell's response to the mix.

## DISCUSSION

### Odor Representations in Piriform Cortex

Olfactory perception is initiated by the recognition of odorants by a large repertoire of receptors in the sensory epithelium. Distributed neural activity in the nose is converted into a segregated, coarse chemotopic map in the olfactory bulb. This transformation results from the convergence of like axons, each bearing the same receptor, on a given glomerulus. This organization combines the robustness of a redundant, spatially unbiased sampling system in the nose with the economy of a condensed spatial representation in the olfactory bulb. Optical imaging of responses in the cortex reveals a second transformation in which odorants activate a subpopulation of neurons distributed across the piriform cortex. The piriform therefore discards spatial segregation as well as chemotopy and returns to a highly dispersed organization in which different odorants activate unique ensembles of cortical neurons.

An individual odorant activates an ensemble that consists of 3%–15% of the cells in piriform at low concentration, an observation that implies that a neuron will respond to multiple odorants. Indeed, we observe significant overlap in the responses of individual neurons to structurally dissimilar odorants. These imaging results are consistent with electrophysiological studies showing that individual piriform cells respond to diverse odorants (Rennaker et al., 2007; Litaudon et al., 2003; Yoshida and Mori, 2007; Kadohisa and Wilson, 2006; Poo and Isaacson, 2009). The frequency of responsive cells we observe is in accord with a recent study that employed patch-clamp recordings to sample the odorant-evoked responses of piriform cells (Poo and Isaacson, 2009). This similarity is observed despite the presumed differences in the sensitivity of $Ca^{2+}$ imaging and electrophysiological recording. One implication of these observations is that piriform processing does not generate cells that respond to an odorant with great specificity, the equivalent of olfactory "grandmother cells." Rather, odorants appear to be represented by unique ensembles of active neurons.

A neuron within an ensemble activated by a given odorant responds to multiple dissimilar odorants, but often fails to respond to structurally similar odorants. Thus, piriform cells

possess discontinuous receptive fields that appear fundamentally different from those in neocortical sensory areas. In primary visual cortex, V1, for example, a cell responsive to a given orientation is likely to respond to lines of similar orientation but not to lines of very different orientation (Hubel and Wiesel, 1959).

Neurons in piriform cortex not only exhibit discontinuous receptive fields, but neurons responsive to a given odorant are distributed without apparent spatial preference. As a consequence, cells with widely differing olfactory receptive fields are interspersed. This finding extends previous studies that revealed a distributive odorant representation across the piriform by examining electrophysiological activity and Fos expression (Rennaker et al., 2007; Illig and Haberly, 2003). These studies, however, were unable to address the interspersion of cells with different response properties. Two-photon imaging of odor responses in the dorsal telencephalon of the zebrafish also reveals a dispersed ensemble of active neurons with only small differences in the spatial distribution of cells responsive to different odors (Yaksi et al., 2009).

Although coarse chemotopy exists in the bulb, our data reveal that no correspondence between chemical receptive field and position can be found in the piriform. Rather, individual piriform cells themselves possess discontinuous receptive fields, and no contiguity in response properties is observed among neighbors. These data suggest organizational principles that differ from those of neocortical sensory areas where cells responsive to similar stimulus features are clustered, and response properties vary smoothly across the cortex. The feedforward maps encoding tonotopy in A1, visuotopy in V1, and somatotopy in S1 in mice and other mammals exhibit spatial continuity of neurons responsive to similar stimuli (Woolsey and Walzl, 1942; Talbot and Marshall, 1941; Marshall et al., 1941). However, cells preferring similar orientations in V1 are not clustered in rodents (Ohki et al., 2005). This organization in rodent V1 may reflect a novel strategy for organizing visual information or may simply reflect the small number of cells in the diminutive rodent cortex. In other mammals, cells clustered within a given orientation column have overlapping retinotopic receptive fields. In rodents, however, cells with similar orientation preferences have not been shown to possess overlapping receptive fields. The small rodent V1 may simply not contain multiple cells of a given orientation selectivity and receptive field.

In vision and somatosensation, information central to perception exists in two dimensions in the external world, and a two-dimensional representation is maintained from the peripheral sense organs to the sensory cortices. The identity of olfactory information in the physical world does not have a meaningful representation in two dimensions, and we observe no spatial order in the odorant representations in piriform cortex. The difference between the cortical representation in olfaction and other sensory systems may also reflect the high dimensionality of odorant space compared to other modalities or perhaps the discrete rather than continuous character of odorant detection within that space.

## The Representation of Odorant Mixes

The patterns of neural activity observed upon exposure to a mix of odorants reveal that the representations in piriform do not simply sum the component representations nor are they dominated by synergistic responses. Rather, the overriding feature observed with mixes is a suppression of activity in cells responsive to the individual odorants presented alone. Electrophysiological studies have similarly described mixture suppression as well as facilitation of odorant-evoked responses in individual neurons in the piriform (Wilson, 2003; Yoshida and Mori, 2007). This suppression may in part be attributed to inhibitory interneurons in layer 1 that exhibit nonselective excitation (Poo and Isaacson, 2009). Mixture suppression has also been observed in mitral cells but is more specific than the pervasive suppression we observe in piriform (Davison and Katz, 2007). In the zebrafish, the mixture suppression observed in the telencephalon exceeds the suppression recorded in mitral cells of the bulb (Yaksi et al., 2009). Our data suggest that suppression may serve an essential normalization function, maintaining a limited number of active neurons independent of the complexity of an odorant. This may be important given that natural odorants often consist of multiple molecular components each capable of exciting 10% of the cortical neurons when presented alone. Summation without suppression would result in global activity in cortex resulting in massively overlapping patterns of neural activity, a phenomenon that could degrade discriminatory power.

The pattern of active neurons in response to a mix of odorants differs from the representations of the individual components. Despite these differences, behavioral studies demonstrate that rodents retain the ability to detect the individual odorant components in a mix (Linster and Smith, 1999; Dreumont-Boudreau et al., 2006; Wiltrout et al., 2003). The observation that mix representations do not reflect the sum of component activities suggests that the recognition of individual odorants in a mix does not require the complete ensemble of active neurons elicited by an odorant in isolation.

## How Are Odorant Representations in the Piriform Generated?

Individual odorants interact with multiple receptors, resulting in the activation of multiple glomeruli in the olfactory bulb. If the identity of an odorant is defined by the combination of active glomeruli, then the olfactory system must integrate activity across multiple glomeruli. Integration could be accomplished by both the olfactory bulb and piriform cortex. Piriform cells responsive to a given odorant are distributed without apparent spatial preference. However, imaging studies of the bulb reveal a coarse chemotopy; glomeruli responsive to related odorants are spatially segregated but are interspersed among glomeruli of diverse specificities (Lin et al., 2006; Takahashi et al., 2004; Ingarashi and Mori, 2005; Soucy et al. 2009). The distributive representation in the piriform no longer exhibits any chemotopic organization and is therefore likely to result from a reorganization of olfactory information downstream of the bulb.

Individual piriform cells respond to structurally dissimilar odorants, whereas mitral cells respond with far more stringent selectivity (Davison and Katz, 2007). These observations suggest that information from different glomeruli converge upon individual piriform cells downstream of the bulb (Franks and Isaacson, 2006). Additional evidence for convergence is revealed by

a subpopulation of cells responsive only to a mix of odorants but not to the components. Although this synergy may reflect the activation of a single glomerulus by each component of the mix, the finding of synergy with structurally dissimilar odorants renders this possibility less likely. Thus, the observation that individual piriform cells respond to dissimilar odorants and the finding of synergistic activation of neurons by a mix of dissimilar odorants provide evidence for the convergence of distinct glomerular inputs on a single cortical neuron.

We cannot at present discern whether the projections of different mitral cells upon piriform neurons are random or determined. Since an odorant can activate as many as 100 glomeruli, the distributed pattern of neural activity we observe in piriform could result from the spatially segregated input of 100 classes of mitral cells to discrete regions of piriform, which in aggregate innervate the entire cortical space. Although determined, this pattern of innervation could give the appearance of a random distribution. Alternatively, mitral cells from individual glomeruli may indeed project diffusely and randomly to innervate cortical neurons such that each pyramidal cell receives a random and unique combination of glomerular inputs. Preliminary data from our laboratory (R. Datta, D. Sosulsky, D., and R.A., unpublished data) indicate that projections from a single glomerulus are not spatially segregated but broadly innervate the piriform, a finding consistent with models of random convergence.

We have generated a model that invokes random convergent excitatory inputs from mitral cells onto piriform neurons (Figure S12; Supplemental Discussion). In the model, each pyramidal cell also receives a second inhibitory set of inputs mediated by local neurons in the piriform. The population of piriform cells, each connected with an independent combination of glomeruli, thus samples possible combinations in an unbiased manner. This random model affords an explanation for the dispersed responses to odorants and reliably predicts the quantitative results of our imaging experiments (Figure S12).

If the connections from bulb to cortex are indeed random, then the representation of the quality of an odorant or its valence in the piriform must be imposed by experience, rendering the piriform a purely associative cortex. Odorants, however, can elicit innate behavioral responses suggesting that a second area of the brain must receive stereotyped and determined inputs from the olfactory bulb. A similar organization may be operative in insects where stereotyped connections to the protocerebrum mediate innate olfactory responses, whereas it has been argued that random inputs to the mushroom body mediate learned olfactory behavior (Jortner et al., 2007; Murthy et al., 2008).

The consequence of random mitral cell inputs on piriform cells could produce sensory representations such that cells responsive to a given odorant are dispersed rather than segregated and exhibit discontinuous receptive fields. This differs from the representations observed in sensory neocortices that encode vision, touch, or sound. Rather, the piriform may be more reminiscent of the hippocampus, another three-layered cortical area. Place cells in hippocampus, for example, exhibit no apparent relationship between their position in brain space and their receptive field in external space (O'Keefe et al., 1998; Redish et al., 2001), a possible intriguing parallel between the representations in piriform cortex and hippocampus.

## EXPERIMENTAL PROCEDURES

### Animal Subjects

Imaging experiments were carried out in 188 animals. All data shown were acquired in male B6CBAF1 mice obtained from Jackson Laboratories. Experiments were also conducted in females and a different strain (C57BL/6, also from Jackson), with similar results. The ages of experimental animals ranged from 3 to 10 weeks. The data presented were obtained in animals anesthetized with ketamine/xylazine (100 mg/kg ketamine and 10 mg/kg xylazine initial dose; 30 mg/kg ketamine every 20–30 min maintenance doses). Experiments using urethane (1.5 mg/g) yielded similar results in B6CBAF1 mice. All subjects were treated in accordance with institutional guidelines of the Columbia University Medical Center.

### Surgical Preparation

Subjects were allowed to eat and drink freely until the start of the experiment. Under anesthesia, an incision was made rostrocaudally from the mouth to the ear across the cheek, and the skin was retracted to expose the masseter muscle. The superficial temporal vein was severed by cauterization, after which the zygomatic bone extending from the squamosal bone to just posterior to the eye was removed with fine scissors. A dorsoventral incision was subsequently made in the masseter muscle halfway between the eye and ear, penetrating all the way to the outer surface of the mandible, using the cautery. The upper portion of the mandible including the coronoid and condyloid processes was then removed with fine scissors. The temporalis muscle was afterward disconnected from the skull along the temporal ridge and retracted. Completion of these steps exposed the ventral lateral surface of the skull with minimal bleeding, and the targeted imaging site was clearly visible through the skull at the intersection of the LOT and MCA. A headpost was then fixed to the dorsal surface of the skull using dental acrylic (Coltene/Whaledent) and a water-impermeable barrier constructed around the surgical site with silicone sealant (WPI). A small craniotomy, usually 1 mm dorsoventrally by 2–3 mm rostrocaudally, was then drilled over the piriform. After removal of the skull, the silicone well surrounding the craniotomy was filled with artificial cerebral spinal fluid (ACSF; 125 mM NaCl, 5 mM KCl, 10 mM glucose, 10 mM HEPES, 2 mM $CaCl_2$, 2 mM $MgSO_4$) at all times. The internal temperature of subjects was maintained at 37.0°C using a feedback-controlled heating pad (FST), and subjects were hydrated by continuous intraperitoneal injection of normal saline supplemented with glucose.

### Dye Injections

All imaging was carried out using an Ultima two-photon microscope (Prairie Technologies). Injections of calcium-sensitive dye were made under two-photon microscopy in a manner similar to that previously described by other groups, with a few modifications (Stosiek et al., 2003; Ohki et al., 2005). Oregon Green 488 BAPTA-1 AM was dissolved in DMSO with 20% Pluronic F-127 to produce a concentration of 0.8 mM, and this solution was diluted 1/40 with standard pipette solution containing red dye (150 mM NaCl, 2.5 mM KCl, 10 mM HEPES, 20 μM Alexa Fluor 594; dyes from Molecular Probes). This dye solution was pressure injected into one or more locations of piriform, 100–130 μm deep, through glass micropipettes with tip diameter of 3 μm. The red dye in the pipette solution allowed us to visualize our injections, which sometimes failed due to clogging. We achieved good labeling of thousands of cells in layer 2 after successfully injecting the dye 50–100 times in 100–200 ms puffs spaced at 5 s intervals. We calculate that injections yielding the widest expanses of well-labeled cells totaled tens of nl based upon estimated volumes that the dye solution occupied in our pipettes before and after injecting. Functional imaging was not performed until 1 hr after the injections were complete to allow the calcium dye to fully load the cells. The craniotomy was covered with 2% agarose (TypeIII-A, Sigma) in ACSF and a fragment of No. 0 glass coverslip, cut to fit inside the silicone sealant well, to suppress brain movement due to breathing and vascular pulsation.

### Functional Imaging

All odorants were obtained from Sigma (except mouse urine, which we collected, and TMT, which we obtained from Pherotech) and of the highest purity available. The odorants were diluted in DPG to bring them to

approximately equal concentrations in air as estimated using their published vapor pressures. For mixture experiments, the odorants were mixed in liquid phase at the same concentrations as those used for individual presentation. Subjects were stimulated with odorants using a custom-made olfactometer (manifolds, valves, and valve controllers purchased from Automate). Medical air from a tank was filtered through activated charcoal and hydrated by bubbling through water prior to its delivery to the olfactometer. For each trial, the targeted cells were initially imaged for 2 s under a constant flow of clean air to obtain a measure of baseline fluorescence and noise. The airflow was switched to odorant-laced air for 1 s and then back to clean air with no change in overall flow rate. Subjects were presented with odorants or controls—air or di(propylene glycol) (DPG)—in a random order for 10 to 20 trials for each set of targeted cells. Preliminary experiments demonstrated that the duration of calcium signals elicited by odorants varied across cells but that the longest responses dissipated by 15 s. The presentation of consecutive stimuli was therefore separated by at least 15 s. Two-photon imaging was carried out with either a Nikon LWD 16X .80W or Nikon FLUOR 40X .80W objective. The excitation wavelength was set to 810 nm, and the fluorescence emission was filtered with Chroma's 580 dcxr dichroic and hq525/70 m-2p bandpass filter. Acquisition of time series of images was programmed (165 × 165 pixel region of interest; 2.0 μs dwell time per pixel) to allow collection of images at ~6 Hz for durations of 5–6 s. After functional imaging was complete for a given site, a picture of the blood vessels at the surface of the cortex was acquired to assist in the montage of multiple sites.

### Image Analysis

The imaging data were analyzed using custom software written in Matlab. To reduce movement noise before analysis, individual images in each trial time series were aligned relative to each other, and data from different trials and conditions were also subsequently aligned, using an autocorrelation routine (Figure S2). The autocorrelation routine incorporated the Matlab function normxcorr2, which computes the normalized cross-correlation between a template matrix and a comparison matrix. The template matrix was the first image in an individual t-series for single t-series alignment, the cross-image average of the (usually) first trial t-series for multiple trial alignment, and the cross-trial average of the first condition of multiple condition alignment. Multiple methods were used to assess odorant-evoked responses, yielding similar results. A simple cell-based approach was used to construct the response maps presented in the paper (Figure S1). The raw, unfiltered images at each time point were averaged across all trial t-series for each stimulus condition. Cell bodies within the imaged region were automatically identified using a cross-condition, cross-trial average image as the template. The pixels within automatically identified cell bodies were then averaged so that each cell's response to each condition was represented by a single series of average fluorescence values over time. These average fluorescence values were converted into relative fluorescence changes (ΔF/F) by subtracting then dividing each series by the mean value obtained during the first 2 s of imaging when no odorant was presented. To normalize for differences in noise across the population of cells, each series was further divided by the standard deviation over this 2 s baseline period, a step that was only undertaken for the assessment of significant responses and is not reflected in any of the other presented data. The response of a cell to a given odorant was then calculated as the mean normalized ΔF/F during the 2 s after the onset of odorant presentation. A given cell was considered significantly responding to a given odorant if its response was greater than the average plus 2.58 times the standard deviation response to air across the entire cell population. The ΔF/F traces of responsive cells were visually inspected and compared with those of nonresponsive cells to assess the method's sensitivity and accuracy in identifying cells with odorant-evoked changes in fluorescence.

### Random Connectivity Model

Simulations of the model were run using custom software written in Matlab. An odorant activated N out of 1000 glomeruli/mitral cells (G/Ms), representing input from 1000 different receptors and disregarding differences between glomeruli or mitral cells receiving the same input. G/M responses to an odorant were assigned values according to an exponential distribution. Each piriform cell (P) was connected through excitatory connections with $C_{ex}$ G/Ms and through inhibitory connections with $C_{in}$ G/Ms. $C_{ex}$ and $C_{in}$ could differ. The magnitude of an individual excitatory input equaled the response of its G/M and the magnitude of an individual inhibitory input equaled the response of its G/M times a factor, $M_{in}$. Inhibitory connections from a G/M to a P were assumed to pass through inhibitory neurons in the piriform. If, for example, N = 50, $C_{ex}$ = 150, $C_{in}$ = 300, and $M_{in}$ = 0.55, then G/Ms 1 to 50 out of 1000 would be activated and any P would receive excitatory input from any of these falling within its randomly assigned combination of 150 connected excitatory G/Ms and inhibitory input from any of these falling within its randomly assigned combination of 300 connected inhibitory G/Ms. The value of its inhibitory inputs would be reduced by a factor of 0.55. For each cell, the total inhibitory input was summed and subtracted from the total, summed excitatory input, yielding the net excitatory or inhibitory effect of the odorant on the cell. If this value exceeded an arbitrary threshold of net excitation (T), then the cell was deemed responsive. Simulations were run for 1000 Ps with different values of N, $C_{ex}$, $C_{in}$, $M_{in}$, and T to identify those combinations of parameter values producing the observed results.

## SUPPLEMENTAL DATA

Supplemental Data include 12 figures followed by a brief supplemental discussion describing the model of random connectivity and can be found with this article online at http://www.cell.com/neuron/supplemental/S0896-6273(09)00684-9.

## ACKNOWLEDGMENTS

We thank Larry Abbott, Cori Bargmann, Randy Bruno, Charles Gilbert, Adam Hantman, Tom Jessell, Eric Kandel, Tony Movshon, Karel Svoboda, and members of the Axel lab for comments on the manuscript; Dara Sosulski for assistance with early experiments; Ming Zhong for technical assistance with later experiments; Monica Mendelsohn and Jennifer Kirkland for help with the mice; Larry Abbott for help in development of the random connectivity model; Bob Datta and John Rafter for assistance with two-photon microscopy; Kenichi Ohki and Clay Reid for providing advice concerning calcium dye injections; Gary Johnson for making some of the hardware used in these experiments; and Phyllis Kisloff, Miriam Gutierrez, and Adriana Nemes for assistance with general laboratory concerns and the preparation of this manuscript. Financial support was provided by the Howard Hughes Medical Institute and the Mathers Foundation.

Accepted: September 1, 2009
Published: September 23, 2009

## REFERENCES

Araneda, R.C., Peterlin, Z., Zhang, X., Chesler, A., and Firestein, S. (2004). A pharmacological profile of the aldehyde receptor repertoire in the rat olfactory epithelium. J. Physiol. *555*, 743–756.

Belluschio, L., and Katz, L.C. (2001). Symmetry, stereotypy, and topography of odorant representations in mouse olfactory bulbs. J. Neurosci. *21*, 2113–2122.

Bozza, T., McGann, J.P., Mombaerts, P., and Wachoiak, M. (2004). *In vivo* imaging of neuronal activity by targeted expression of a genetically encoded probe in the mouse. Neuron *42*, 9–21.

Buck, L., and Axel, R. (1991). A novel multigene family may encode odorant receptors: a molecular basis for odor recognition. Cell *65*, 175–187.

Davison, I.G., and Katz, L.C. (2007). Sparse and selective odor coding by mitral/tufted neurons in the main olfactory bulb. J. Neurosci. *27*, 2091–2101.

Denk, W., Strickler, J.H., and Webb, W.W. (1990). Two-photon laser scanning fluorescence microscopy. Science *248*, 73–76.

Dreumont-Boudreau, S.E., Dingle, R.N., Alcolado, G.M., and LoLordo, V.M. (2006). An olfactory biconditional discrimination in the mouse. Physiol. Behav. *87*, 634–640.

Franks, K.M., and Isaacson, J.S. (2006). Strong single-fiber sensory inputs to olfactory cortex: implications for olfactory coding. Neuron *49*, 357–363.

Godfrey, P.A., Malnic, B., and Buck, L.B. (2004). The mouse olfactory receptor gene family. Proc. Natl. Acad. Sci. USA *101*, 2156–2161.

Hubel, D.H., and Wiesel, T.N. (1959). Receptive fields of single neurons in the cat's striate cortex. J. Physiol. *148*, 574–591.

Illig, K.R., and Haberly, L.B. (2003). Odor-evoked activity is spatially distributed in piriform cortex. J. Comp. Neurol. *457*, 361–373.

Ingarashi, K.M., and Mori, K. (2005). Spatial representations of hydrocarbon odorants in the ventrolateral zones of the rat olfactory bulb. J. Neurophysiol. *93*, 1007–1019.

Johnson, B.A., and Leon, M. (2000). Modular representations of odorants in the glomerular layer of the rat olfactory bulb and the effects of stimulus concentration. J. Comp. Neurol. *422*, 496–509.

Jortner, R.A., Farivar, S.S., and Laurent, G. (2007). A simple connectivity scheme for space coding in an olfactory system. J. Neurosci. *27*, 1659–1669.

Kadohisa, M., and Wilson, D.A. (2006). Separate encoding of identity and similarity of complex familiar odors in piriform cortex. Proc. Natl. Acad. Sci. USA *103*, 15206–15211.

Kerr, J.N.D., de Kock, C.P.J., Greenberg, D.S., Bruno, R.M., Sakmann, B., and Helmchen, F. (2007). Spatial organization of neuronal population responses in layer 2/3 of rat barrel cortex. J. Neurosci. *27*, 13316–13328.

Lin, D.Y., Shea, S.D., and Katz, L.C. (2006). Representation of natural stimuli in the rodent main olfactory bulb. Neuron *50*, 937–949.

Linster, C., and Smith, B.H. (1999). Generalization between binary odor mixtures and their compounds in the rat. Physiol. Behav. *66*, 701–707.

Litaudon, P., Amat, C., Bertrand, B., Vigouroux, M., and Buonviso, N. (2003). Piriform cortex heterogeneity revealed by cellular responses to odours. Eur. J. Neurosci. *17*, 2457–2461.

Malnic, B., Hirono, J., Sato, T., and Buck, L.B. (1999). Combinatorial receptor codes for odors. Cell *96*, 713–723.

Marshall, W.H., Woolsey, C.N., and Bard, P. (1941). Observations on cortical somatic sensory mechanisms of cat and monkey. J. Neurophysiol. *4*, 1–24.

Meister, M., and Bonhoeffer, T. (2001). Tuning and topography in an odor map on the rat olfactory bulb. J. Neurosci. *21*, 1351–1360.

Mombaerts, P., Wang, F., Dulac, C., Chao, S.K., Nemes, A., Mendelsohn, M., Edmondson, J., and Axel, R. (1996). Visualizing an olfactory sensory map. Cell *87*, 675–686.

Murthy, M., Fiete, I., and Laurent, G. (2008). Testing odor response stereotypy in the Drosophila mushroom body. Neuron *59*, 839–1052.

Ohki, K., Chung, S., Ch'ng, Y.H., Kara, P., and Reid, R.C. (2005). Functional imaging with cellular resolution reveals precise microarchitecture in visual cortex. Nature *433*, 597–603.

Oka, Y., Katada, S., Omura, M., Suwa, M., Yoshihara, Y., and Touhara, K. (2006). Odorant receptor map in the mouse olfactory bulb: in vivo sensitivity and specificity of receptor-defined glomeruli. Neuron *52*, 857–869.

O'Keefe, J., Burgess, N., Donnett, J.G., Jeffrey, K.J., and Maguire, E.A. (1998). Place cells, navigational accuracy, and the human hippocampus. Philos. Trans. R. Soc. Lond. B Biol. Sci. *353*, 1333–1340.

Poo, C., and Isaacson, J.S. (2009). Odor representations in olfactory cortex: "Sparse" coding, global inhibition, and oscillations. Neuron *62*, 850–861.

Price, J.L., and Powell, T.P.S. (1970). The mitral and short axon cells of the olfactory bulb. J. Cell Sci. *7*, 631–691.

Redish, A.D., Battaglia, F.P., Chawla, M.K., Estrom, A.D., Gerrard, J.L., Lipa, P., Rosenzweig, E.S., Worley, P.F., Guzowski, J.F., McNaughton, B.L., and Barnes, C.A. (2001). Independence of firing correlates of anatomically proximate hippocampal pyramidal cells. J. Neurosci. *21*, RC134.

Rennaker, R.L., Chen, C.-F.F., Ruyle, A.M., Sloan, A.M., and Wilson, D.A. (2007). Spatial and temporal distribution of odorant-evoked activity in the piriform cortex. J. Neurosci. *27*, 1534–1542.

Ressler, K.J., Sullivan, S.I., and Buck, L.B. (1993). A zonal organization of odorant receptor gene expression in the olfactory epithelium. Cell *73*, 597–609.

Ressler, K.J., Sullivan, S.L., and Buck, L.B. (1994). Information coding in the olfactory system: evidence for a stereotyped and highly organized epitope map in the olfactory bulb. Cell *79*, 1245–1255.

Rubin, B.D., and Katz, L.C. (1999). Optical imaging of odorant representations in the mammalian olfactory bulb. Neuron *23*, 499–511.

Soucy, E.R., Albeanu, D.F., Fantana, A.L., Murthy, V.N., and Meister, M. (2009). Precision and diversity in an odor map on the olfactory bulb. Nat. Neurosci. *12*, 210–220.

Spors, H., and Grinvald, A. (2002). Spatio-temporal dynamics of odor representations in the mammalian olfactory bulb. Neuron *34*, 301–315.

Stosiek, C., Garaschuk, O., Holthoff, K., and Konnerth, A. (2003). In vivo two-photon imaging of neuronal networks. Proc. Natl. Acad. Sci. USA *100*, 7319–7324.

Sugai, T., Miyazawa, T., Fukuda, M., Yoshimura, H., and Onada, N. (2005). Odor-concentration coding in the guinea pig piriform cortex. Neuroscience *130*, 769–781.

Takahashi, Y.K., Kurosaki, M., Hirono, S., and Mori, K. (2004). Topographic representation of odorant molecular features in the rat olfactory bulb. J. Neurophysiol. *92*, 2413–2427.

Talbot, S.A., and Marshall, W.H. (1941). Physiological studies on neural mechanisms of visual localization and discrimination. Am. J. Ophthalmol. *24*, 1255–1263.

Uchida, N., Takahashi, Y.K., Tanifiuji, M., and Mori, K. (2000). Odor maps in the mammalian olfactory bulb: domain organization and odorant structural features. Nat. Neurosci. *3*, 1035–1043.

Vassar, R., Ngai, J., and Axel, R. (1993). Spatial segregation of odorant receptor expression in the mammalian olfactory epithelium. Cell *74*, 309–318.

Vassar, R., Chao, S.K., Sitcheran, R., Nunez, J.M., Vosshall, L.B., and Axel, R. (1994). Topographic organization of sensory projections to the olfactory bulb. Cell *79*, 981–991.

Wachowiak, M., and Cohen, L.B. (2001). Representations of odorants by receptor neuron input to the mouse olfactory bulb. Neuron *32*, 723–735.

Wilson, D.A. (2003). Rapid experience-induced enhancement in odorant discrimination by anterior piriform cortex neurons. J. Neurophysiol. *90*, 65–72.

Wiltrout, C., Dogra, S., and Linster, C. (2003). Configural and nonconfigural interactions between odorants in binary mixture. Behav. Neurosci. *117*, 236–245.

Woolsey, C.N., and Walzl, E.M. (1942). Topical projection of nerve fibers from local regions of the cochlea to the cerebral cortex of the cat. Bull. Johns Hopkins Hosp. *71*, 315–344.

Xu, F., Liu, N., Kida, I., Rothman, D.L., Hyder, F., and Shepherd, G.M. (2003). Odor maps of aldehydes and esters revealed by functional MRI in the glomerular layer of the mouse olfactory bulb. Proc. Natl. Acad. Sci. USA *100*, 11029–11034.

Yaksi, E., von Saint Paul, F., Niessing, J., Bundschuh, S.T., and Friedrich, R.W. (2009). Transformation of odor representations in target areas of the olfactory bulb. Nat. Neurosci. *12*, 474–482.

Yoshida, I., and Mori, K. (2007). Odorant category profile selectivity of olfactory cortex neurons. J. Neurosci. *27*, 9105–9114.

Zhang, X., and Firestein, S. (2002). The olfactory receptor gene superfamily of the mouse. Nat. Neurosci. *5*, 124–133.